Materials Today Bio 28 (2024) 101162

Contents lists available at ScienceDirect

Materials Today Bio

journal homepage: www.journals.elsevier.com/materials-today-bio

Type I collagen-targeted liposome delivery of Serca2a modulates myocardium calcium homeostasis and reduces cardiac fibrosis induced by myocardial infarction

Wanshi Chen [a,b,1], Lingjuan Liu [a], Ming Tang [c], Jiajin Li [a], Wenjing Yuan [a], Dan Yin [a,b], Yang Cao [b], Jie Tian [a,*]

[a] Department of Cardiology, Ministry of Education Key Laboratory of Child Development and Disorders, National Clinical Research Center for Child Health and Disorders, China International Science and Technology Cooperation Base of Child Development and Critical Disorders, Chongqing Key Laboratory of Paediatrics, National Clinical Key Cardiovascular Specialty, Key Laboratory of Children's Important Organ Development and Diseases of Chongqing Municipal Health Commission, Children's Hospital of Chongqing Medical University, Chongqing, China

[b] Chongqing Key Laboratory of Ultrasound Molecular Imaging, Institute of Ultrasound Imaging, Ultrasound Department of Second Affiliated Hospital, Chongqing Medical University, Chongqing, China

[c] Department of Cardiology, The First Affiliated Hospital of Chongqing Medical University, Chongqing, China

ARTICLE INFO

Keywords:
Nanoparticles
Myocardial infarction
Myocardial fibrosis
Calcium homeostasis
Serca2a

ABSTRACT

Fibrotic scarring and impaired myocardial calcium homeostasis serve as the two main factors in the pathology of heart failure following myocardial infarction (MI), leading to poor prognosis and death in patients. Serca2a is a target of interest in gene therapy for MI-induced heart failure via the regulation of intracellular calcium homeostasis and, subsequently, enhancing myocardial contractility. A recent study also reported that Serca2a ameliorates pulmonary fibrosis by blocking nuclear factor kB (NF-kB)/interleukin-6 (IL-6)-induced (SMAD)/TGF-β signaling activation, while the effect in MI-induced myocardial fibrosis remains to be addressed. Here, we loaded Serca2a plasmids into type 1 collagen-targeting nanoparticles to synthesize the GKWHCTTKFPHHYCLY-Serca2a-Liposome (GSL-NPs) for targeted treatment of myocardial infarction. We showed that GSL-NPs were effectively targeted in the scar area in MI-induced mice within tail-vein delivery for 48 h. Treatment with GSL-NPs improved cardiac functions and shrank fibrotic scars after MI in mice by up-regulating Serca2a. In cardiac fibroblasts, GSL-NPs alleviated hypoxia-induced fibrotic progression partly by inhibiting NF-kB activation. Furthermore, treatment with GSL-NPs protected cardiomyocyte calcium homeostasis and enhanced myocardial contractility during hypoxia. Together, we demonstrate that type I collagen-targeted liposome delivery of Serca2a may benefit patients with myocardial infarction by inhibiting fibrotic scarring as well as modulation of calcium homeostasis.

1. Introduction

Myocardial infarction (MI) induced heart failure serves as the major causes of human death worldwide [1,2]. A significant proportion of cardiomyocytes undergo degeneration and necrosis during MI, resulting in a local deficiency of myocardial contractility in the infarct area [3,4]. In contrast, cardiac fibroblasts secrete large amounts of extracellular matrix, and collagen fibers gather excessively in the myocardium, which aggravates left ventricular systolic dysfunction, myocardial non-contractile scar development, and left ventricular remodeling [5]. Hence, effective restoration of myocardial contractility and amelioration of myocardial fibrosis can enhance cardiac function and minimize the likelihood of adverse cardiovascular events, which is highly significant in treating MI.

The disruption of calcium homeostasis in cardiomyocytes caused by ischemia is considered to be a significant trigger for the impairment of myocardial contractility during MI, which was characterized by the decreased uptake of Ca^{2+} by the endoplasmic reticulum of cardiomyocytes and insufficient rate and amplitude of recovery of cytoplasmic Ca^{2+} concentration during diastole, resulting in insufficient

* Corresponding author.
E-mail address: jietian@cqmu.edu.cn (J. Tian).
[1] These authors contributed equally to this work.

https://doi.org/10.1016/j.mtbio.2024.101162
Received 28 March 2024; Received in revised form 10 July 2024; Accepted 18 July 2024
Available online 27 July 2024

myocardial contractility and delayed myocardial diastole [6,7]. Sarcoplasmic reticulum Ca^{2+}-ATPase 2a (Serca2a) is a vital enzyme in the calcium transport channel to maintain calcium homeostasis in cardiomyocytes [8]. Accumulated studies have reported a significant decrease of Serca2a during MI, leading to intracellular Ca^{2+} overload and contractile dysfunction in mice [9,10]. It has also been demonstrated that Serca2a heterozygous knockout (Serca2a (±) could aggravate in vivo myocardial ischemia/reperfusion (I/R) injury and affect postischemic functional recovery [11]. Conversely, increased Serca2a expression in cardiomyocytes protects heart functions in various experimental animal models, including myocardial infarction, I/R injury, or afterload-induced cardiac hypertrophy mice [7,12–14], showing that Serca2a may serve as a promising therapeutic target against heart failure by maintaining calcium homeostasis and enhancing myocardial contractility. Another possible protective effect of Serca2a in post-myocardial infarction may come from its resistance to myocardial fibrosis. By boosting Serca2a gene delivery in a bleomycin-induced lung fibrosis model, a recent study reported that AAV-mediated Serca2a therapy could reverse pulmonary fibrosis in mice by blocking NF-κB and subsequently inhibiting TGF-β/SMAD2/3 signaling pathway [15]. TGF-β is a solid and robust fibrogenic cytokine which plays a vital role in triggering myocardial fibrosis [16–18]. Although several studies highlight the potential role of Serca2a in inhibiting fibrosis progression by protecting calcium homeostasis and maintaining myocardial contraction [19,20], whether treatment of Serca2a could directly alleviate myocardial fibroblast activation after MI remains to be further addressed.

Despite the success of Serca2a treatment in experimental heart failure, a multinational, randomized, placebo-controlled, double-blind CUPID 2 trial in which 250 patients (aged 18 to 80) with stable chronic HF and reduced ejection fraction received AAV/Serca2a pellet infusion failed to demonstrate an improvement in the time to onset of heart failure when compared to placebo control [21]. Although the factors that led to the failure of this clinical trial are complex, two issues stand out: 1. Biological resistance and potential toxicity of AAV therapy; 2. Limitations in targeting infarct areas. Hence, it is urgent to find highly biosafety and targeted delivery systems for gene therapy at myocardial infarction sites. In this study, we suggest a nanoparticle-based gene therapy regimen for the targeted delivery of Serca2a. After the surgery, we created a gene therapy delivery system that aggressively targets the infarction area of the heart. In our previous study, lipid nanoparticles were modified with corresponding peptides on the surface to provide better targeting for multimodal imaging in a mouse model of myocardial ischemia/reperfusion [22,23]. GKWHCTTKFPHHYCL, a peptide discovered by in vivo phage display technology, consists of 16 amino acids and can be specifically bound to type I collagen (the primary collagen component in fibrotic myocardium), to promote the targeting of nanoparticles in the fibrotic area caused by MI [24,25]. Briefly, this novel and revolutionary platform comprise a core of cationic liposomes loaded with Serca2a and a surface shell of a GKWHCTTKFPHHYCL peptide that targets type 1 collagen. The core of the nanoparticle possesses a high Serca2a loading capacity, which could effectively prevent the degradation of Serca2a in bodily fluids. By injecting tail veins into MI-operated mice, our nanoparticles were preferentially nested and enriched in the post-infarction fibrotic zone by GKWHCTTKFPHHYCL peptide, resulting in the local release of Serca2a from cardiac fibroblasts in the infarction area as well as from nearby cardiomyocytes (Fig. 1). The results of this study demonstrate that our nanoparticle-mediated Serca2a targeting gene delivery system may serve as a promising therapeutic option for patients with myocardial infarction.

2. Materials and methods

2.1. Materials

1,2-dipalmitoyl-sn-glycerol-3-phosphatidylcholine (DPPC), 1,2-stearoyl-sn-glycerol-3-phosphatidyl amino-N- [methoxy (polyethylene glycol)-2000] (DSPE-PEG2000) and cationic cholesterol (DC-Chol) were purchased from Corden Pharma Inc (Liestal, Switzerland). EP-3533 (GKWHCTTKFPHHYCLY, cyclic form) and DSPE-PEG2000-GKWHC TTKFPHHYCLY were synthesized and purified by Xi'an Rui Xi Biotechnology Co. Ltd (Shanghai, China). 1,1′-dioctadecyl-3,3,3′,3′-tetramethylindocarbocyanine perchlorate (DiI), 4′, 6-diamidino-2-phenylindole (DAPI), and 1,1′-dioctadecyl-3,3,3′,3′-tetramethylindotricarbocyanine iodide (DiR) were purchased from Sigma-Aldrich (Saint Louis, MO, USA). Dulbecco's modified Eagle's medium (DMEM), fetal bovine serum (FBS), and trypsin were purchased from Gibco Co. (Carlsbad, CA, USA). Penicillin-streptomycin was purchased from Boost Biotech Co. Cell Counting Kit 8 (CCK-8) was provided by Dojindo Molecular Technologies (Tokyo, Japan). Hydrogen peroxide (H2O2), trichloromethane (CHCl3), and other analytical-grade reagents were purchased from Chongqing Chuandong Chemical (Chongqing, China). The Serca2a plasmid was purchased from GKN Genetics (Shanghai, China).

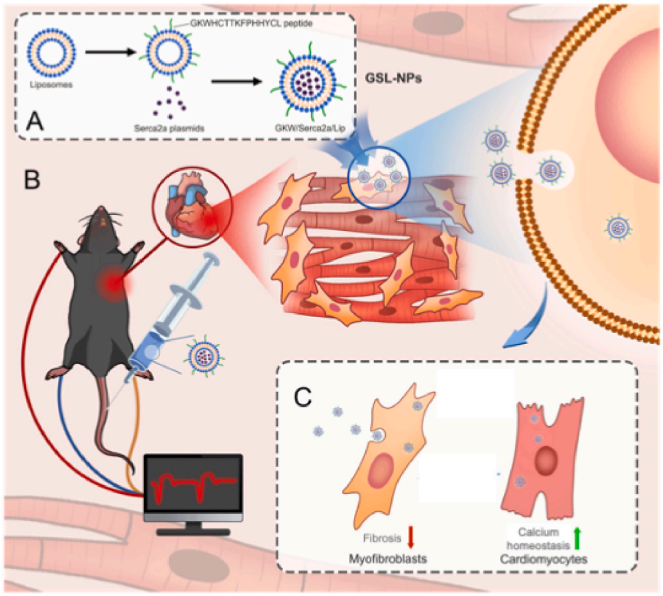

Fig. 1. Schematic illustration of the design of GSL-NPs to treat myocardial infarction in mice.
A: Preparation of cationic lipid nanoparticles, which were prepared with cationic liposomes loaded with Serca2a as the core and type 1 collagen-targeting GKWHCTTKFPHHYCL peptide as the shell on the surface. B: In a mouse myocardial infarction model, the lipid nanoparticles were injected through the tail vein, which could be enriched in the fibrotic area after infarction and thus phagocytosed by cardiomyocytes and myocardial fibroblasts, followed by the release of Serca2a plasmid. C: Serca2a plasmid uptake by cardiac fibroblasts and cardiomyocytes improves myocardial contractility by inhibiting the activation of fibrosis in fibroblasts and protecting calcium homeostasis in cardiomyocytes.

2.2. Synthesis of lipid nanoparticles

1,2-Dipalmitoyl-sn-glycero-3-phosphatidylcholine (DPPC, 10 mg), 1,2-distearoyl-sn-glycero-3-phosphatidylamino-N-[methoxy (polyethylene glycol)-2000] (DSPE-PEG2000, 4 mg) and cationic cholesterol (DC-Chol, 3 mg) were dissolved with 10 ml of trichloromethane (Chongqing Chuandong Chemical, Chongqing China), then the organic solvent was removed using a rotary vacuum evaporator (RE-52A, Yarong, Shanghai, China). The suspension was pulsed and shaken in an ice water bath at 125 W for 8 min using an ultrasonicator (Sonics & Materials Inc., USA). Subsequently, the emulsion was successfully isolated through a series of centrifugation processes in a refrigerated centrifuge at 4 °C, (8000 rpm, 5 min three times) to obtain a homogeneous

nanoscale contrast agent (Liposome nanoparticles, L-NPs). After each centrifugation, 4 ml of phosphate-buffered saline (PBS) was used to wash for further studies. Then we co-incubated the Serca2a plasmid with the previously prepared L-NPS for 30 min to obtain the liposomal nanoparticle material with Serca2a (Serca2a-Liposome nanoparticles, SL-NPs). To synthesize nanoparticles with COL1-targeting properties, GKWHCTTKFPHHYCLY peptide was recruited and labeled on SL-NPs using a typical carbodiimide method. Briefly, replace DSPE with DSPE-PEG2000-GKWHCTTKFPHHYCLY (4 mg, Xi'an Ruixi Biotechnology Co., Ltd., Xi'an, China) in the initial step and gradually synthesize targeted nanoparticles (GKWHCTTKFPHHYCLY-Serca2a-Liposome, GSL-NPs, Fig. 2A) according to the process described above. Finally, the diameter and distribution of the nano-contrast agents were observed by light microscopy (Olympus, Tokyo, Japan) and confocal laser scanning microscopy (A1R–Si; Nikon, Tokyo, Japan). Transmission electron microscopy (TEM) (H-7500; Hitachi, Tokyo, Japan) was used to observed the morphology and microstructure of the nanoparticles.

2.3. Nanoparticle loading gene amount and DNase I protection assay

Equal amounts of Serca2a plasmids were randomly prepared in 10 copies. Different amounts of lipid nanoparticles made as described above were added into Serca2a plasmids respectively, then incubated for 1 h to synthesize lipid nanoparticles containing Serca2a in different concentrations (Lipid nanoparticles/Serca2a = 0–9/1). DNase I protection experiments were also performed to investigate the ability of

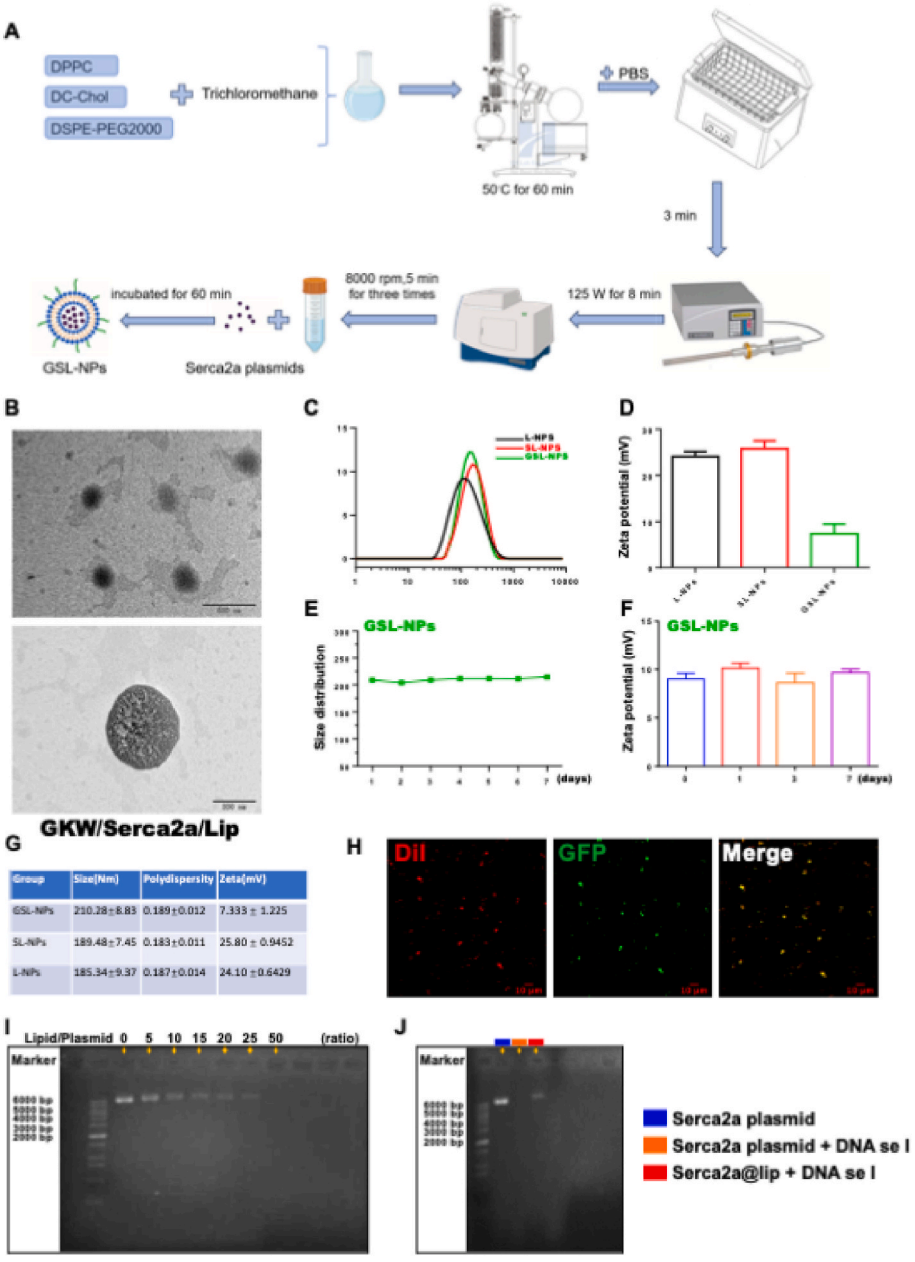

Fig. 2. Physical characteristics of lipid nanoparticles. (a) Schematic diagram of GSL-NPs preparation; (b) TEM images of GSL-NPs (scale = 500 nm; Scale = 200 nm). (c,d) Diameter (c), zeta potential (d) of SL-NPs, GSL-NPs, and L-NPs measured by DLS in PBS. (e,f) The changes in particle size (e) and zeta potential (f) of GSL-NPs nanoparticles on different days were measured. (g) A statistical table including particle size, polydispersity, and zeta potential of GSL-NPs, SL-NPs, and L-NPs is shown. (h) Confocal laser scanning micro-graphs: Dil-labeled GSL-NPs (red), GFP-labeled Serca2a (green), and merge. (i) The free Serca2a plasmid was detected by agarose gel at about 6000bp. The gradient mass ratio of GL-NPs and Serca2a was used to make GL-NPs: Serca2a = 0:1, 5:1, 10:1, 15:1, 20:1, 25:1, 50:1 on 2 % agarose gel. (j) Nanoparticles protect against DNA Se I-derived degradation of Serca2a plasmid.

nanoparticles to protect Serca2a from DNase I degradation. Serca2a or GSL-NPs complexes were exposed to PBS or DNase I digestion and incubated at 37 °C for 60 min, after which the samples were subjected to agarose gel electrophoresis.

2.4. Cell culture, cell viability, and TUNEL staining

Cardiac fibroblasts and H9C2 cells were cultured in Dulbecco's modified Eagle medium (DMEM) supplemented with 10 % fetal bovine serum (Gibco, Invitrogen, Grand Island, NY, USA) at 37 °C and 5 % CO_2. Cardiac fibroblasts and H9C2 cells were loaded into 96-well plates at 5 × 10^4 cells per well for. For cytotoxicity assays, cardiac fibroblasts, and H9C2 cells were treated with GSL-NPs (0, 0.1, 0.2, 0.4, 0.8, 1.0 mg/ml) for 24 and 48h. Cell viability was measured by a CCK-8, and a microplate reader (Multiskan MK33; Thermolab Systems, Helsinki, Finland) was used to detect the optical density at a wavelength of 450 nm.

For TUNEL staining, after washing with PBS for 3 × 5min, the cell slivers were treated with 0.3 % Triton drilling for 5 min, then washed again with PBS for 3 × 5min. TUNEL staining solution (Meilunbio) was prepared according to the instructions, then added into each cell slide and incubated in a 37 °C water bath for 60 min. After incubation, DAPI was treated after PBS wash, and the slices were sealed with an anti-quench sealing tablet and observed under Confocal Microscope.

Uptake of GKW/Serca2a/Lip by cardiac fibroblasts and H9C2 cells.

The uptake of GSL-NPs by cardiac fibroblasts and H9C2 cells was assessed by laser confocal microscopy (Nikon, Japan). Under laser confocal microscopy, cardiac fibroblasts and H9C2 cells were cultured on confocal dishes with culture medium for 24 h and then exposed to a hypoxic environment (37 °C and 1 % oxygen) for 24 h of incubation. Next, cardiac fibroblasts and H9C2 cells were exposed to DMEM containing Dil-labeled GSL-NPs (200 μg/ml, 1.5 ml/well) for 1, 2, 3, or 4 h under standard cell culture conditions, respectively. Cells were washed three times with ice-cold PBS and fixed with 4 % paraformaldehyde for 10 min at 37 °C. Then, the plates were rewashed three times with PBS, and the nuclei of the samples were stained with DAPI dye for 5 min. Subsequently, fluorescent images were obtained by laser confocal microscopy.

2.5. Biosafety detection of lipid nanoparticles in vivo

Specific pathogen-free (SPF) C57BL/6 mice (18–22 g) were purchased from the Experimental Animal Center of Chongqing Medical University (Chongqing, China). All experimental animal procedures were performed in accordance with the guidelines of the Ethics Committee of Chongqing Medical University Laboratory Animal Center.

To assess the in vivo toxicity of GSL-NPs, mice were randomly divided into the following five groups based on nanoparticle treatment time: sham, 7-day, 14-day, and 28-day experimental groups (n = 5 per group). By tail vein injection, the control group was treated with saline (200 μL), and other groups were treated with GSL-NPs (dose: 1.0 mg/kg, 1.0 mg/ml). Throughout the testing period, abnormal reactions, deaths, and the time of their occurrence were observed and recorded. At different time points, whole blood was collected from the heart, part was used for routine blood tests, and part was separated from the serum for biochemical analysis. At the end of the experiment, all mice were sacrificed, and the major organs (heart, liver, spleen, lungs, and kidneys) were taken for histological analysis using hematoxylin and eosin staining (H&E).

2.6. Establishment of mouse MI model and experimental process

A total of 48 male C57BL/6 mice were randomly assigned into 5 groups as follows: a sham group (n = 8), MI group (n = 10), Lip group (MI + Liposome injection, n = 10), Serca2a/Lip group (MI + Serca2a/Lip injection, n = 10), and GKW/Serca2a/Lip group (MI + GKW/Serca2a/Lip injection, n = 10). To establish the MI model, C57BL/6J mice were anesthetized by intraperitoneal injection of pentobarbital (60 mg/kg), followed by mechanical ventilation at a respiratory rate of 200 breaths/min and a tidal volume of 0.15 ml. After the mice were anesthetized, a left thoracotomy was performed, and a sternal retractor was placed to separate the rib cage and expose the heart. The left anterior descending artery (LAD) was ligated with 8-0 wire in both MI and the treatment groups. Mice in the sham group underwent the same procedure without LAD ligation. After the ligation, the muscle, fascia, and skin were sequentially sutured in layers with 5-0 sutures. The three different treatment strategies (Lip, Serca2a/Lip, GKW/Serca2a/Lip, 1 mg/kg, 1 mg/ml)) were administered intravenously in mice every two days for 28 days, starting the second day after MI modeling. At the end of the experiment, all mice were killed with a lethal dose of sodium pentobarbital (3 %; 80 mg/kg). Blood samples were collected in dry test tubes without anticoagulant to obtain serum. Myocardial tissue was immediately excised and rapidly dissected on ice. All samples were stored for further use.

2.7. In vivo fluorescence assay

A fluorescent system (CRi Inc, Woburn, MA, USA) was used to study the distribution of GSL-NPs in MI mice. A total of 12 mice were randomly divided into 4 groups (n = 3 for each group): MI-operated plus SL-NPs or GSL-NPs administration group was injected with DiR-labeled SL-NPs (1.0 mg/kg, 1.0 mg/ml) or GSL-NPs (1.0 mg/kg, 1.0 mg/ml) through the tail vein 14 days after MI operation. After the sham operation, the sham-operated plus SL-NPs or GSL-NPs administration group was injected with the same doses of SL-NPs or GSL-NPs. After 1, 6, 12, 24, and 48 h of injection, the mice were placed in front of the camera for image analysis of DiR dye and calculating the relative fluorescence intensity, respectively.

2.8. Echocardiography

After anesthetized with inhaled isoflurane via a facemask, the mice were subjected to transthoracic echocardiography using a Vevo 3100 (Visual Sonics Inc., Toronto, ON, Canada) equipped with an MS550 transducer (22–55 MHz). Left heart systolic functions, including ejection fraction (EF), fractional shortening (FS), left ventricular systolic diameter (LVSD) and left ventricular diastolic diameter (LVDD), were detected as we previously described [26].

2.9. Western blot analysis

Total proteins were isolated from the heart tissues of mice and cardiac fibroblasts. 20 mg of each heart tissue from the left ventricular was lysed with RIPA buffer containing protease inhibitor cocktails (Sigma) using Benchmark Bead blast 24 tissue homogenizer (Benchmark scientific). Protein samples (20 μg/lane) were separated by SDS-PAGE and transferred to a nitrocellulose filter membrane (Millipore Sigma). Antibodies recruited in the present study were shown as follows: anti-Serca2a (1:5000; Abcam, ab150435), anti-β-actin (1:500; Santacruz, SC-130657), anti-COL1 (1:1000; Bioss, bs-10423R), anti-α-SMA (1:3000; Abcam, ab124964), anti-GAPDH (1:5000; Abcam, ab8245), anti–NF–κB p65 (1:1000; Cell Signaling Technology, 8242), anti-p–NF–κB p65 (1:1000; Abcam, ab76302), anti-*p*-SMAD2/3 (1:1000; Abcam, ab272332), anti-t-SMAD2/3 (1:1000; Abcam, ab202445), anti-IL-1β (1:1000; Abcam, ab283818), anti-NLRP3 (1:1000; Abcam, ab263899), anti-TGF-β1 (1:1000; Abcam, ab215715).

2.10. RNA isolation and quantitative RT-PCR analysis

Total RNA samples from rat lung tissues were isolated and purified using RNAiso Reagent (Takara Japan) according to the manufacturer's protocol. The mRNA levels were measured using the TB Green Premix Ex Taq (TaKaRa, Tokyo, Japan) and the Thermal Cycler Dice Real-Time

System (Bio-rad, Hercules, CA, United States). The following PCR condition was applied: 95 °C for 3 min, 40 cycles at 95 °C for 10s, and 62 °C for the 30s followed by 62 °C 10s. Following are the sequences of the primers: forward: CTCAAGGAGAGATGGGGCTC; reverse: CAATCACAAGTTCCAGCAAGGT.

2.11. Immunofluorescence staining and histological analysis

Heart tissues from Sham/MI mice (treated with Serca2a/Lip or GKW/Serca2a/Lip 24hrs before sacrifice) were sectioned into 5 μm slices by frozen tissue sectioning, then blocked with 0.1 % Triton X-100 and immunostaining blocking solution at room temperature for 1 h. After 3 washes with PBS, the slices were incubated with anti-COL1 (1:50; Bioss, bs-10423R) at 4 °C overnight, then incubated with FITC conjugated affineur goat anti-rabbit IgG (1:100; Proteintech, SA00003-2) at room temperature for 1 h. Finally, the sections were stained with DAPI before being imaged under a fluorescence microscope (Eclipse Ti–U, Nikon Corporation, Tokyo, Japan) at an excitation wavelength of 405 nm for nuclei and 488 nm for COL1. For cardiac fibrosis immunofluorescence, cells were seeded into a cell slide and then grown to a 60–70 % density. After being fixed with 4 % paraformaldehyde for 15 min, a standardized immunofluorescence staining procedure and confocal microscopy detection were administered as described above. Anti-α-SMA antibody (1:100; Abcam, ab124964) and FITC conjugated affineur goat anti-rabbit IgG (1:100; Proteintech, SA00003-2) was used additionally.

To demonstrate the correlation between Serca2a and COL1 in cardiac fibroblasts, COL1-positive cells in the left ventricle of different groups of mice were isolated using antibody magnetic bead (For tissue dissociation: Multi tissue Dissociation Kit 2, 130-110-203, Miltenyi Biotech; For cell sorting: Anti-Rabbit IgG MicroBeads, 130-048-602, Miltenyi Biotech) according to the manufacturer's protocol, and then immunofluorescence co-staining of Serca2a and COL1 was performed using the antibody described above. After incubated with FITC conjugated affineur goat anti-rabbit IgG (1:100; Proteintech, SA00003-2) and Cy3 conjugated affineur goat anti-mouse IgG (1:100; Proteintech, SA00009-1) for 1 h, confocal microscopy detection was administered in the cardiac fibroblasts isolated from each group of mice. Line-intensity profiles of Serca2a, COL1 and DAPI in each single cell acquired from MI + Serca2a/Lip group and MI + GKW/Serca2a/Lip group were measured using imageJ as we described in the previous study [27].

For histological analysis, heart tissues were fixed in 4 % paraformaldehyde for 48 h, dehydrated and embedded in paraffin, sectioned at 4-μm thickness, then mounted on glass slides. Masson's trichrome staining was used to assess the extent of fibrosis in cardiac muscle.

2.12. Detection of calcium transient in adult mouse cardiomyocytes and neonatal cardiomyocytes, and H9C2s

Adult mouse cardiomyocytes were extracted and cultured according to a published protocol [28]. EDTA buffer was injected into the right ventricle, the aorta was clipped, and the heart was cut off. Next, EDTA buffer was injected into the left ventricle and replaced with perfusion buffer. Then, collagenase was injected into the left 5 ventricles until the digestion was finished. We tore the heart to the full extent with tweezers, mixed it for 1 min, and finally terminated digestion with a stop buffer. The extracted cardiomyocytes were filtered with a 100 μm filter net and collected with centrifuge tubes. With compound calcium fluid, the filtrate was settled three times by gravity for 20 min each time, and the precipitates were collected and reselected with a culture medium. Viable cardiomyocytes from each group were incubated with Fluo-4 AM working solution (2 μM, Biotechnology, China) in a 37 °C incubator for fluorescence probe loading and then observed using a spinning-disk confocal microscope (SpinSR, Olympus, Japan). In order to reflect the calcium change of sarcoplasmic reticulum (SR), the calcium probe fluorescence intensity of individual cardiomyocytes before and after stimulation was obtained by quickly adding 10 mmol/L caffeine to the cells under confocal observation.

To determine the effect of GSL-NPs on spontaneous calcium transients of cardio-myocytes, neonatal mouse ventricular myocytes were isolated from 2-day-old C57BL/6 mice by enzymatic digestion with 0.05 % trypsin and 0.015 % collagenase then planted in 35 mm confocal dishes as we previously described [29]. After being treated with GSL-NPs (1 mg/ml) or scrambled NPs for 4 h, neonatal cardiomyocytes were washed with PBS 3 times and then exposure to hypoxia (1%O_2) for 24 h. Ca^{2+} transient was determined using Fluo-4 AM working solution according to the procedure described above. Whole-cell fluorescent images of each cardiomyocyte were recorded 40 times in 10 s by confocal microscope (SpinSR, Olympus, Japan).

To demonstrate the effect of exogenous stimuli on sarcoplasmic reticulum calcium pumps, H9C2 cells were recruited and labeled with Fura-2/AM probes to determine intracellular calcium changes. Briefly, cells were inoculated in a 6-well plate, cultured to approximately 90 % growth density, removed from the medium, and washed twice with extracellular fluid. After that, extracellular fluid containing 1 μm Fura-2/AM and 0.025 % F-127 (Invitrogen) was added to the cell. Then, darkly incubated at 37 °C for 40 min. Next, washing the cells once with extracellular fluid and three times with calcium-free extracellular fluid, adding intracellular solution with 10 mg/ml digitonin to the cells and incubating at 37 °C for 5 min to permeabilize the cell membrane. Finally, the cells were washed twice with intracellular fluid, scraped, and re-sustained into a 96-well plate with 200 μl intracellular fluid. Setting up the microplate reader to read the fluorescence intensity at the excitation wavelength of 340 nm and emission wavelength of 510 nm. Caffeine with a final concentration of 2 mM was added into a 96-well plate as an agonist by automatic sample feeder.

2.13. Statistical analysis

All data were represented of at least 3 independent experiments and expressed as mean ± SEM, and the group size 'n' refers to biological replicates, not technical replicates. The normal distribution of each data was evaluated for normal distribution using the Shapiro-Wilk test, and $P > 0.05$ indicated the normally distributed. To identify group differences, we used Student's t-test for two groups and one-way analysis of variance (ANOVA) followed by Tukey post-hoc test when comparing more than two groups. The survival rate was presented as a Kaplan–Meier curve and compared by the log-rank test. $P < 0.05$ was considered statistically significant. All the statistical analysis were performed in GraphPad Prism 8.0 software (San Diego, CA, USA).

3. Results

3.1. GSL-NPs exhibit stable physical characteristics with high biosafety and biocompatibility

Transmission electron microscopy detection showed that GSL-NPs were spherical with uniform size and regular morphology (Fig. 2B). Then we determined the physical properties of the nanoparticles, including GSL-NPs, SL-NPs, and L-NPs. As a result, they all showed good dispersibility via the Malvern particle size meter and zeta surface potential detector (1. GSL-NPs, average particle size: 210.28 ± 8.83 nm, zeta potential: 7.33 ± 1.225, PDI: 0.189 ± 0.012; 2. SL-NPs, average particle size: 189.48 ± 7.45 nm, zeta potential: 25.8 ± 0.9452, PDI: 0.183 ± 0.012; 3. L-NPs, average particle size: 185.34 ± 9.37 nm, zeta potential: 24.10 ± 0.6429, PDI: 0.187 ± 0.014; Fig. 2C, D, G). In addition, no significant potential or particle size changes were observed in the nanoparticles during 7 consecutive days of testing (Fig. 2E and F). Using a laser confocal microscope, we showed that GFP-labeled Serca2a plasmids (green signal) were well co-localized to Dil-labeled nanoparticles (red signal), showing a successful linkage of lipid nanoparticles and plasmid genes in our study (Fig. 2H). In order to measure the gene

loading of lipid nanoparticles, we co-incubated lipid nanoparticles and plasmid genes in different ratios for 1 h. As shown in Fig. 2I, as the ratio of lipid nanoparticles to plasmid increased, the levels of free plasmid decreased, and the saturation concentration was reached when the lipid/plasmid ratio exceeded 25/1. Owing that DNA Se I degrades DNA and is widely present in organisms, naked plasmid DNA cannot be efficiently delivered to target tissues and exert gene therapy effects. To test whether GSL-NPs could protect against DNA Se I-derived degradation, we incubated DNA plasmid with DNA Se I in vitro. We found that the naked Serca2a plasmid was significantly degraded within 30 min, while loaded with nanoparticles reversed this effect as detected by agarose gel (Fig. 2J), indicating that Serca2a plasmids were well protected against DNA Se I by lipid nanoparticles.

To verify the biosafety of GSL-NPs, we performed serum biochemical and pathological measurements in C57BL/6 mice and cell viability assays in cardiac fibroblasts and H9C2s. Specifically, we measured the cellular activity of cardiac fibroblasts and H9C2s after treatment with GSL-NPs for 24 or 48 h, respectively, using the cck-8 assay, which showed no significant decrease in cell viability, and both were above 90 % even 48 h after 1 mg/ml of GSL-NPs administration (Fig. 3A and B). TUNEL assays further demonstrated that GSL-NPs did not cause significant cell death at a dose of 2 mg/ml (Fig. 3C and D). To evaluate the in

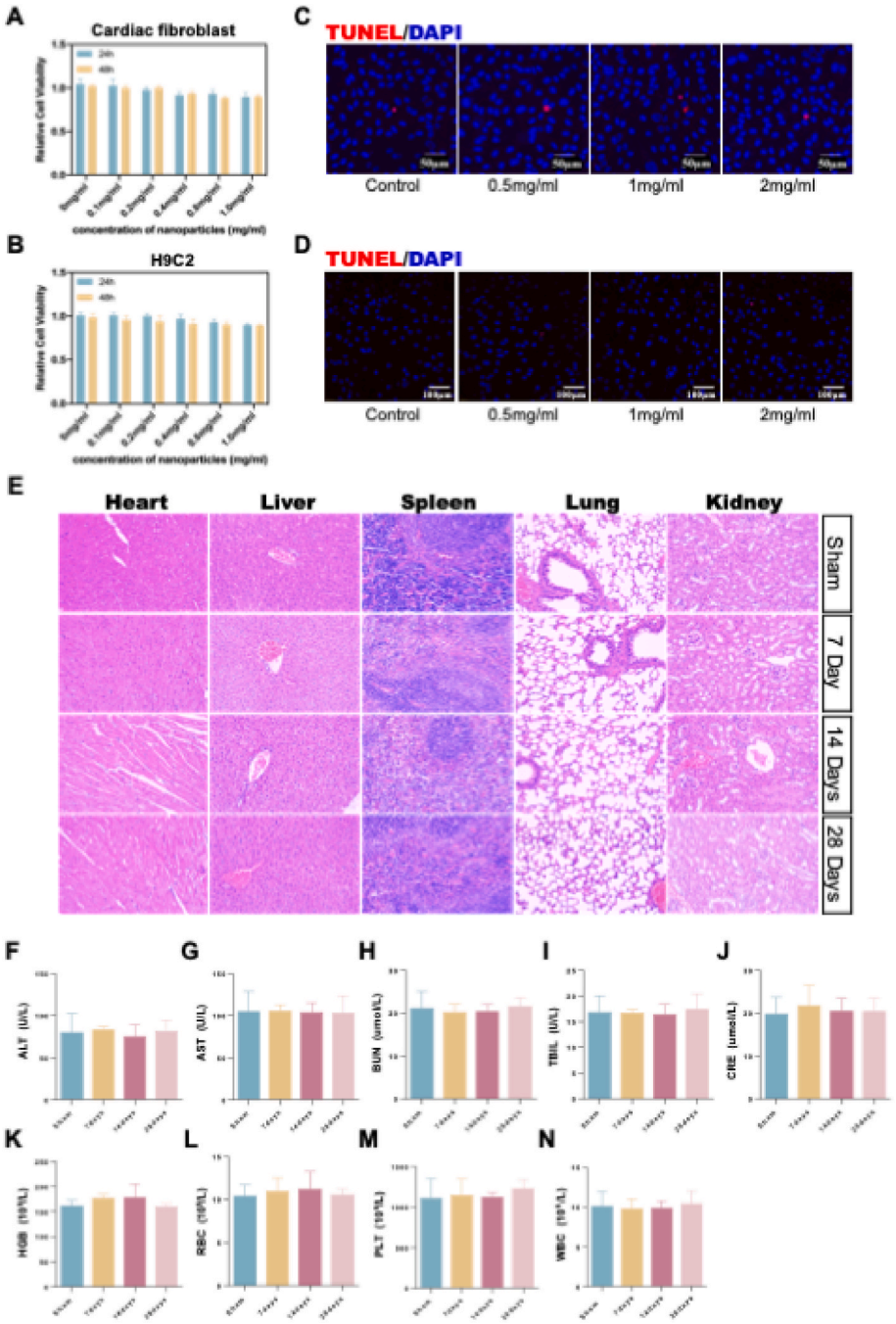

Fig. 3. The biosafety of GSL-NPs in vivo and in vitro. (a,b) The cell viability of normal cardiac fibroblasts (a) and H9C2s (b) treated with different doses and time points of nanoparticles. (c,d) TUNEL staining of normal cardiac fibroblasts (c) and H9C2s (d) treated with different doses of nanoparticles. (e) Representative H&E-stained sections from the heart, liver, spleen, lung, and kidney of each group. (f–n) Serum levels of alanine aminotransferase (ALT), aspartate aminotransferase (AST), blood urea nitrogen (BUN), creatinine (CRE), Total bilirubin (TBIL), hemoglobin (HGB), red blood cells (RBC), platelets (PLT) and white blood cells (WBC) from the different groups.

vivo biosafety of lipid nanoparticles, mice were treated with GSL-NPs (1.0 mg/kg through tail vein) once every two days for 28 consecutive days, then serum biochemical and pathological measurements were performed at day 0, 7, 14, and 28. As shown in Fig. 3E, no significant changes or damage were observed in the major organs of mice at each time point, indicating its low toxicity and biocompatibility in mice. We also found no differences in serum levels via groups including red blood cells (RBC), white blood cells (WBC), platelets (PLT) and hemoglobin (HGB), alanine aminotransferase (ALT), aspartate aminotransferase (AST), blood urea nitrogen (BUN) and creatinine (CRE), indicating that GSL-NPs did not cause additional damage to the physiological functions of mice (Fig. 3F–N).

To verify the phagocytosis of nanoparticles in vitro, we co-incubated GSL-NPs with normal cardiac fibroblasts and H9C2s for 1, 2, 3, or 4 h under standard cell culture conditions, respectively. As shown by immunofluorescence confocal microscopy, the cellular phagocytosis of GSL-NPs began to rise significantly at 2 h of incubation. It reached saturation at 4 h of incubation both in cardiac fibroblasts and H9C2s (Figs. S1A and B). The above results demonstrate that we have successfully synthesized a liposome-loaded nanoparticle plasmid DNA platform with high biosafety and biocompatibility that can efficiently load Serca2a plasmids into cells and protect them from degradation in

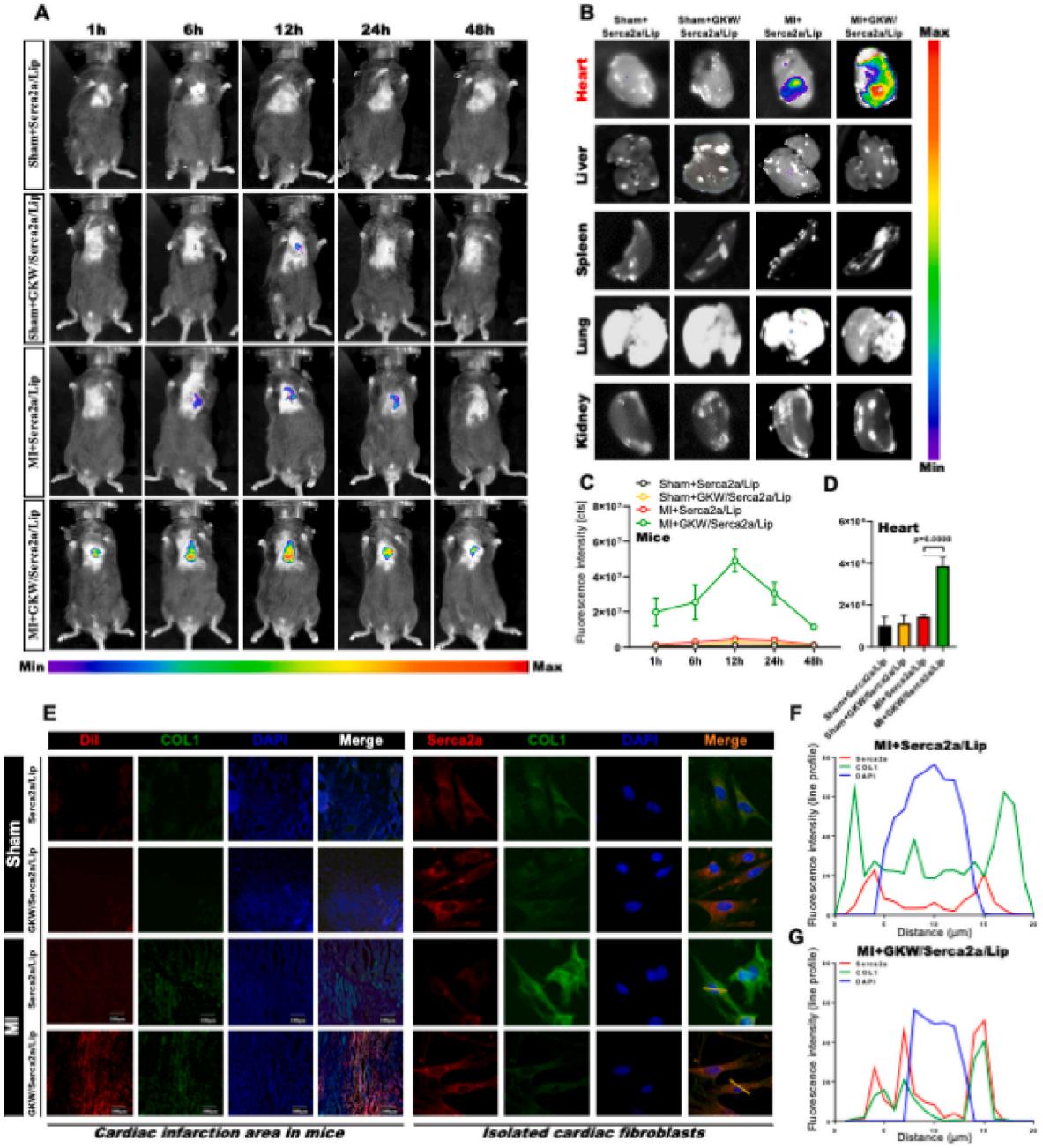

Fig. 4. GSL-NPs are targeted to the infarct area of MI mice by interacting with type 1 collagen fibers. (a, b) Representative in vivo fluorescence images from the different groups of mice (a) and their main organs (b). (c) Quantifications of fluorescence intensity in each group of mice at different time points within 48 h' observation. (d) Quantifications of fluorescence intensity in heart tissues of mice at 48 h after tail vein injection. (e) Representative immunofluorescent images of heart tissues and isolated cardiac fibroblasts in each group of mice are shown. Dil served as fluorescent labeling of nanoparticles. (f, g) Visualization of linear fluorescence intensity (yellow lines in Fig. 4E) between Serca2a and COL1 in MI + Serca2a/lip group (h) group and MI + Gkw/Serca2a/lip group are shown, respectively.

vivo, providing a basis for subsequent administration.

3.2. GSL-NPs were enriched at the site of the myocardial infarction scar by linking with type I collagen of cardiac fibroblasts

To compare the targeted enrichment ability of SL-NPs and GSL-NPs in the heart, we performed in vivo fluorescence detection in sham-operated or MI-operated mice, respectively. As to sham-operated mice, after being injected with each nanoparticle by tail vein, no significant enrichment was detected in the SL-NPs group and GSL-NPs group within 48 h of observation; As to MI-operated mice, the SL-NPs group showed no significant fluorescent signals after tail vein injection within 48 h, while the GSL-NPs group exhibited apparently fluorescent signals at the infarct area of the heart from 1 h to 48 h after tail vein injection, peaking at 12 h and remaining enriched at 48 h (Fig. 4A–C). After 48 h, we sacrificed the mice and examined the major organs of each group, and found that the fluorescence intensity of the heart tissue in the MI-operated plus GSL-NPs injection group was significantly higher than that in the MI-operated plus SL-NPs injection group; On the contrary, there was no significant difference in the fluorescence intensity of the

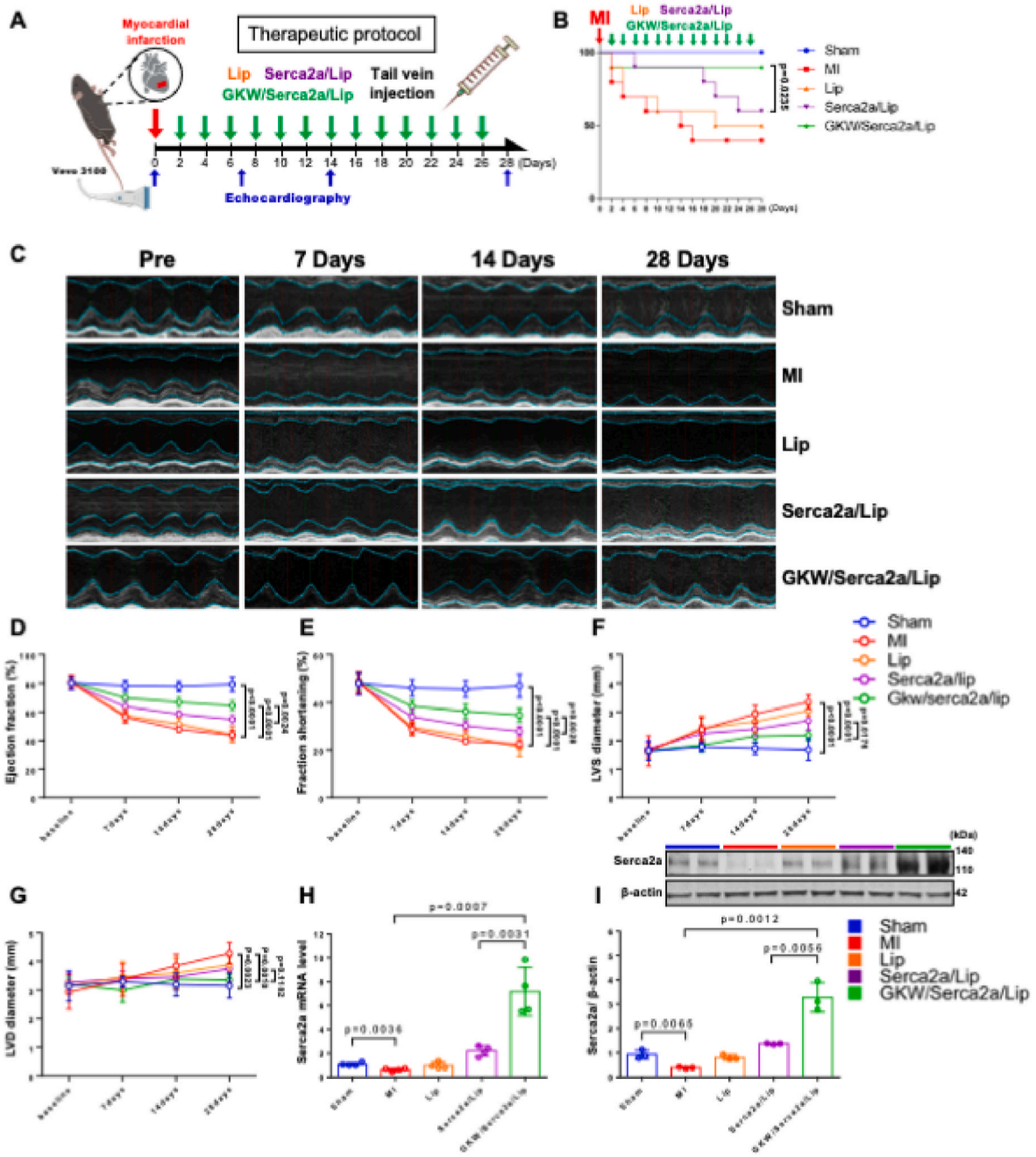

Fig. 5. Delivery of GSL-NPs protects against MI-induced heart failure in mice (a) Schematic of the experimental design to assess the therapeutic efficacy of GSL-NPs in the MI-induced mice. Mice who received a MI surgery were randomly assigned to receive 1 mg/kg L-NPs, SL-NPs, or GSL-NPs once every two days for 28 days; Echocardiographic measurements were performed on days 1,7,14 and 28. (b) Kaplan-Meier survival curves in different groups within 28 days' observation. (c) Representative images for measuring left ventricular systolic function at each time point from the different groups are shown. (d) Ejection fraction, (e) fractional shortening, (f) LVS diameter, and (g) LVD diameter were measured from the different groups, respectively. (h, i) Serca2a mRNA (h) and protein levels (i) from the heart tissues of mice via different groups were measured. L-NPs, lipid nanoparticles; SL-NPs, Serca2a/lipid nanoparticles; GSL-NPs, GKWHCTTKFPHHYCL/Serca2a/lipid nanoparticles.

sham-operated mice regardless of the injected nanoparticles (Fig. 4B–D).

To demonstrate whether nanoparticles accumulate in the infarcted area, we examined frozen sections of heart tissue from each group of mice 12 h after tail vein injection. In sham-operated mice, there is no significant nanoparticles enrichment in both SL-NPs and GSL-NPs group (Red signal, Fig. 4E), consistent with the results observed from the in vivo fluorescence assays. In MI-operated mice, we observed significant activation of type I collagen fibers (Green signal, Fig. 4E) and significantly more nanoparticles in the GSL-NPs-treated group than in the SL-NPs-treated group. In order to observe the changes of Serca2a and COL1 at the single-cell level, we further dissociated the left ventricle of mice in each group then sorted out COL1-positive cells for immunofluorescence confocal imaging. Compared with the MI + Serca2a/Lip group, MI + GKW/Serca2a/Lip group showed a higher Serca2a fluorescence intensity, which was accompanied by a lower COL1 fluorescence intensity (Fig. 4E). Intriguingly, there was a significant correlation between Serca2a and COL1 in the GSL-NPs treated group regardless of whether they experienced MI operation (orange signal in the Merge image, Fig. 4E), but not in the SL-NPs treated group. Linear fluorescence intensity measurements further demonstrated the significant correlation between Serca2a and COL1 in MI + GSL-NPs group, but not in MI + SL-NPs group (Fig. 4F and G). The above results showed that GSL-NPs could enriched in the heart of MI mice by interacting with type 1 collagen fibers in the infarct area.

3.3. Delivery of GSL-Np protects against MI-induced heart failure in mice

To evaluate the therapeutic effect of GSL-NPs on experimental MI, mice in each group were treated once every two days with 1 mg/kg L-NPs, SL-NPs, or GSL-NPs, respectively. The left ventricular function was detected by using echocardiography at day 7, 14 and 28 (Fig. 5A). During the 28-day treatment period, GSL-NPs-treated mice showed a higher survival rate than SL-NPs-treated mice after MI operation (Fig. 5B). MI surgery resulted in significant weight loss and lower basal heart rate in mice within 28 days, which was significantly alleviated by GSL-NPs treatment (Figs. S2A and B). Seven days after the MI model was established, the EF values and FS values were significantly decreased (EF: 78.42 ± 1.598 % vs. 56.35 ± 1.838 %, $P < 0.001$; FS: 46.12 ± 1.499 % vs. 28.72 ± 1.163 %, $P < 0.001$; Fig. 5C, D, E) in MI group versus Sham group, accompanied by the upregulation of LVSD (1.774 ± 0.06622 mm vs. 2.390 ± 0.1894 mm, $P < 0.05$; Fig. 5F). Both treatments of SL-NPs and GSL-NPs attenuate the MI-induced dysfunction in mice (EF: 63.90 ± 2.030 % [Serca2a/Lip, $P < 0.05$] and 70.06 ± 1.314 % [GKW/Serca2a/Lip, $P < 0.001$] vs. 56.35 ± 1.838 % [MI]; FS: 33.95 ± 1.404 % [Serca2a/Lip, $P < 0.05$] and 38.49 ± 1.077 % [GKW/Serca2a/Lip, $P < 0.001$] vs. 28.72 ± 1.163 % [MI]; LVSD: 2.250 ± 0.1240 mm [Serca2a/Lip, $P = 0.5545$] and 1.839 ± 0.1043 mm [GKW/Serca2a/Lip, $P < 0.05$] vs. 2.390 ± 0.1894 mm [MI]; Fig. 5D, E, F), whereas GSL-NPs treatment group showed a more significant protective effect compared with the SL-NPs treatment group ($P < 0.05$). Similar and more substantial changes, including EF, FS, and LVSD, were detected at day 14 and 28 of treatment via groups (Fig. 5D, E, F). Moreover, treatment with GSL-NPs for 28 days significantly alleviates MI-induced upregulation of LVDD, while treatment with SL-NPs did not (3.740 ± 0.2074 mm [Serca2a/Lip, $P = 0.0758$] and 3.354 ± 0.07490 mm [GKW/Serca2a/Lip, $P = 0.001$] vs. 4.287 ± 0.1698 mm [MI]; Fig. 5G). The above results showed that treatment with GSL-NPs provides a sustained and more efficient cardioprotective effect in mice than the non-targeted Serca2a-loaded nanoparticles within 28 days.

We further detected the levels of Serca2a in the LV tissues of mice after 28 days by performing qRT-PCR and Western blotting. As shown in Fig. 5H, the mRNA levels of Serca2a were impaired in the MI group as compared with the sham group, while administered with GSL-NPs apparently increased the transcriptional levels of Serca2a in the heart ($P < 0.001$). A similar activation at the protein level was demonstrated by western blotting ($P < 0.001$; Fig. 5I). Furthermore, we noticed more significant upregulation of Serca2a mRNA levels as well as protein levels in the GSL-NPs treatment group compared to the SL-NPs treatment group (Fig. 5H and I), indicating that GSL-NPs could load more Serca2a plasmids into the heart tissues of mice than SL-NPs after a same dose of tail vein injection.

3.4. GSL-NPs attenuate the activation of cardiac fibrosis in MI-induced mice

To evaluate whether treatment with GSL-NPs attenuates myocardial fibrosis after the MI operation, we performed heart Masson staining in each group of mice after 28 days. As shown in Fig. 6A and B, the Masson positive area in the MI group was significantly increased versus the sham group, which was significantly decreased by GSL-NPs administration. Immunofluorescent staining of COL1 also confirmed the remission of fibrosis in the GSL-NPs treatment group when compared with the MI group ($P < 0.01$) and SL-NPs treatment group ($P < 0.05$), showing a stronger enrichment and anti-fibrotic capacity of GKW/Serca2a/Lip on the fibrotic region than Serca2a/Lip (Fig. 6A–C). The protein levels of COL1 and α-SMA in the heart tissues of mice were increased 28 days after the MI procedure, which was significantly decreased by treatment with GSL-NPs (Fig. 6D, E, F), showing an exaggerated antifibrogenic capacity in vivo. To further elucidate the anti-fibrotic ability of nanoparticles in cardiac fibroblasts, we pretreated cells with L-NPs, SL-NPs, and GSL-NPs, respectively, for 4 h before exposure to hypoxia (1%O_2 for 24 h) and then washed with PBS for 3 times before immunofluorescent staining; As a result, GSL-NPs exhibited better anti-fibrosis ability than SL-NPs in cardiac fibroblasts by immunofluorescence (Fig. 6G and H). Moreover, hypoxia exposure resulted in down-regulation of Serca2a, while administration of GSL-NPs significantly up-regulated Serca2a protein levels in cardiac fibroblasts (Fig. 6I and J). The expression levels of COL1 and α-SMA in each treatment group of cardiac fibroblasts further confirmed the better anti-fibrotic effect of GSL-NPs than SL-NPs (Fig. 6K, L, M), which was consistent with the results observed in immunofluorescent staining. To further demonstrate the inhibitory effect of GSL-NPs on NFKB signaling pathway and its downstream TGF-β fibrotic pathway and inflammatory signals, we measured the expression levels of NF-κB, p- NF-κB, and its downstream signaling including TGF-β1, *p*-SMAD2/3, t-SMAD2/3, NLRP3 and IL-1β in cardiac fibroblasts after treated with different nanoparticles. We found that treatment with GSL-NPs significantly inhibits hypoxia-triggered activation of NF-κB signaling pathway (Fig. 6N and O), as well as its downstream TGF-β fibrotic pathway (Fig. 6N–P, Q) and inflammatory signals including NLRP3 and IL-1β (Fig. 6N–R, S), which are generally considered to be involved in the formation of NF-κB signaling mediated cardiac fibrosis.' [15,30,31] Overall, the present data support three conclusions: (1) Treatment with Serca2a attenuates the activation of fibrosis in MI-induced mice and hypoxia-induced cardiac fibroblasts; (2) GSL-NPs shows stronger anti-fibrosis capacity than SL-NPs both in vivo and in vitro; (3) Serca2a may probably attenuate cardiac fibrosis partly through blocking NF-κB and its downstream signaling pathways.

3.5. GSL-NPs ameliorate calcium homeostasis during MI and hypoxia

To determine the protective effect of GKW/Serca2a/Lip on calcium homeostasis in MI-operated mice, we isolated left ventricular myocytes from each group. We evaluated basal Ca^{2+} concentrations as well as Caffeine-triggered Ca^{2+} changes using Fluo-4 calcium fluorescence staining. We found that Caffeine-triggered Ca^{2+} changes of myocytes in the MI group was significantly lower than that in the control group, which was significantly increased by GSL-NPs administration, showing that fibrotic region-targeted delivery of Serca2a also rescues MI-induced myocardial SR calcium release injury (Fig. 7A and B). Then, we recruited neonatal mouse cardiomyocytes and pre-treated them with GSL-NPs before exposure to hypoxia to determine the effect of GSL-NPs on spontaneous calcium transients in cardiomyocytes in vitro. We found

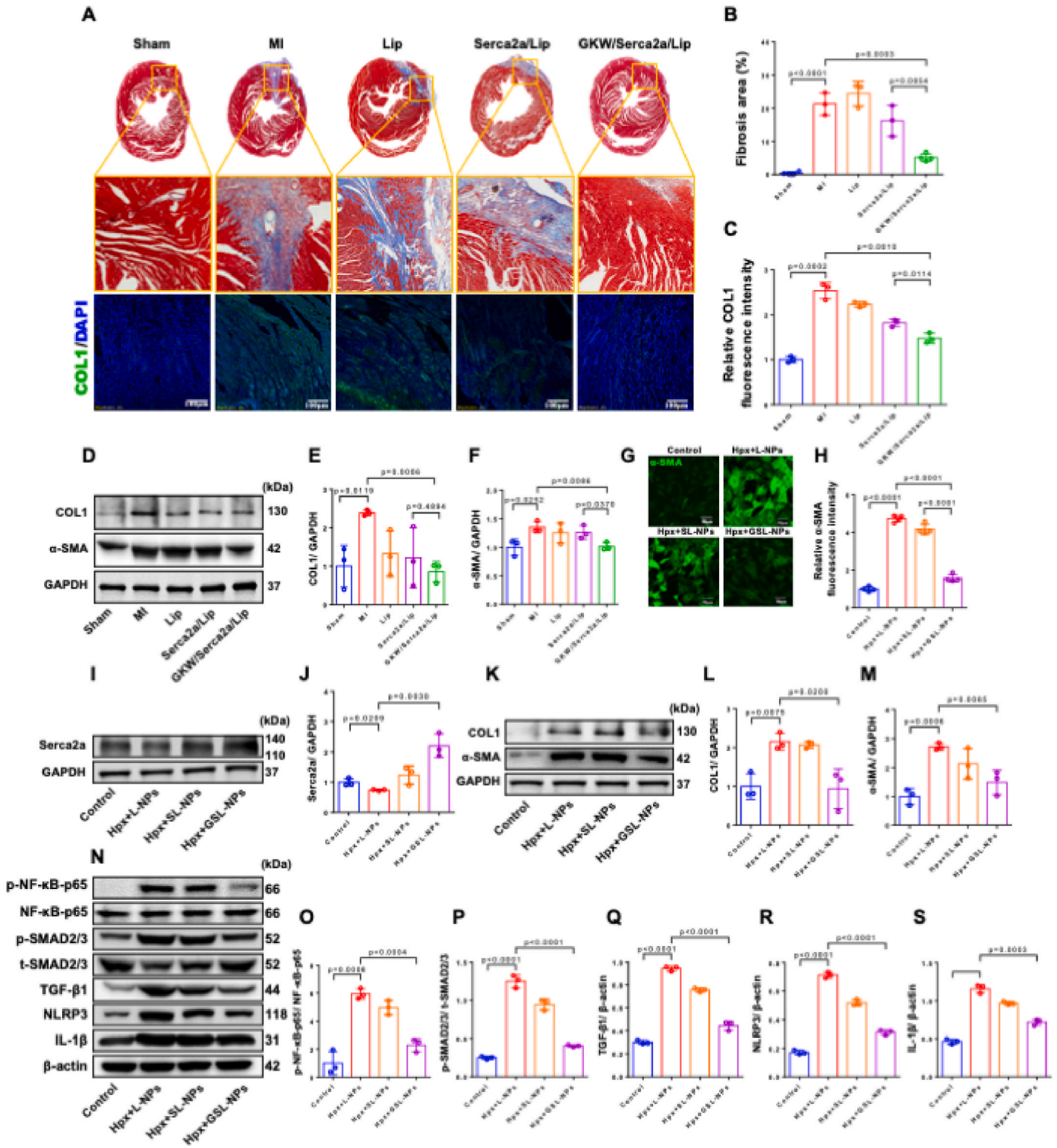

Fig. 6. Delivery of GSL-NPs attenuates MI-induced cardiac fibrosis via down-regulation of NF-κB signaling pathways. (a) Representative images of Masson staining and COL1 immunofluorescence staining from the different groups. Bar = 100 μm (b,c) Quantifications of scar area (b) and COL1 fluorescence intensity (c) based on Masson staining and immunofluorescence staining. (d–f) The protein levels of COL1 and α-SMA in the heart tissues of mice via different groups were measured. (g) Representative immunofluorescent images of α-SMA from cardiac fibroblasts after exposure to 1 % O_2 in each group. Bar = 50 μm. (h) The fluorescence intensity of α-SMA from the different groups was quantified. (i,j) The protein levels of Serca2a in the cardiac fibroblasts via different groups were measured. (k–m) The protein levels of COL1 and α-SMA in the cardiac fibroblasts via different groups were measured. (n–s) The protein levels of p- NF-κB-p65, NF-κB-p65, *p*-SMAD2/3, t-SMAD2/3, TGF-β1, NLRP3 and IL-1β in the cardiac fibroblasts via different groups were measured.

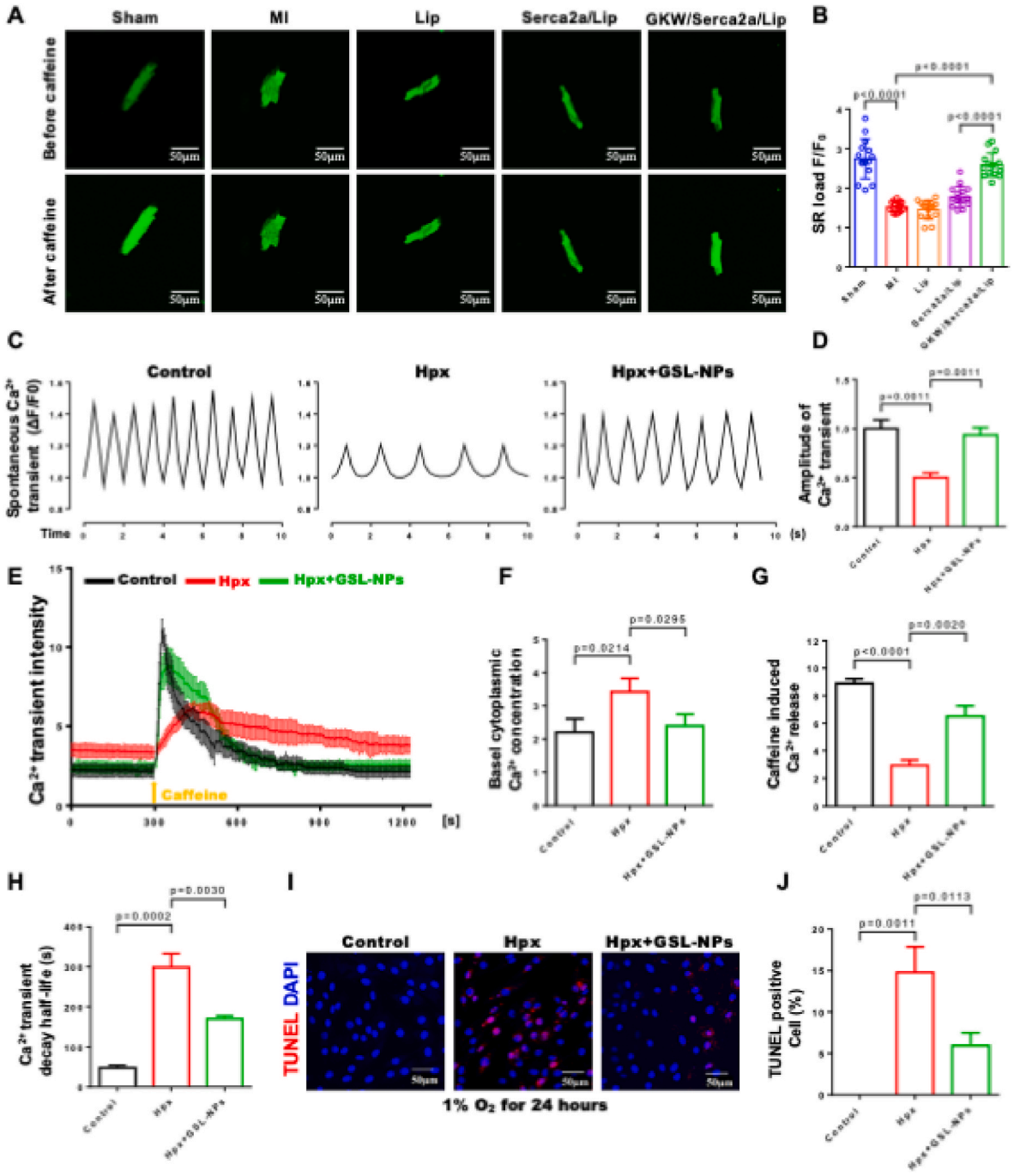

Fig. 7. Delivery of GSL-NPs maintains cardiomyocyte calcium homeostasis during MI. (a, b) (a) Representative images of calcium release from sarcoplasmic reticulum triggered by caffeine in isolated single ventricular myocytes and (b) the changes of relative calcium fluorescence intensity in sarcoplasmic reticulum were evaluated. n = 18 cells from 3 mice. (c–d) Representative calcium transient curve (c) and quantification of amplitude (d) in neonatal cardiomyocytes are shown. (e–h) A calcium transient experiment is used to reflect the level of agonist-induced sarcoplasmic reticulum calcium release and recycling in H9C2s. (e) Intracellular calcium concentration visualization curves and (f) basal calcium intensity, (g) histone-triggered calcium release, and (h) sarcoplasmic reticulum calcium transient decay half-life are shown. (i, j) (i) Representative images of TUNEL staining and (j) the ratio of TUNEL -positive/total H9C2s are shown.

that hypoxia caused disruption of calcium homeostasis in neonatal cardiomyocytes, which was effectively ameliorated by GSL-NPs treatment (Fig. 7C and D). To further demonstrate the role of GSL-NPs in exogenous calcium stimulation, we recruited anoxic H9C2 models and found that treatment with GSL-NPs alleviates hypoxia-induced basal calcium overload (Fig. 7E and F) and simultaneously protects the SR capacity in cells under Caffeine stimulation (Fig. 7E–G, H). Finally, hypoxic damage to cardiomyocytes leads to apoptosis of cardiomyocytes and aggravates heart failure [32–34]. Using TUNEL staining we further confirmed that GSL-NPs treatment protected H9C2s from apoptosis caused by hypoxia (1%O_2 for 24 h, Fig. 7I and J). The above results showed that in addition to anti-fibrotic ability, GSL-NPs could also protect hypoxia-induced cardiomyocyte impairment via modulation of intracellular calcium homeostasis during MI.

4. Discussion

In the present study, we successfully implemented a nanoparticle-

based gene therapy regimen in MI mice through targeted delivery of Serca2a. We demonstrated that GSL-NPs are significantly enriched in the mouse heart by binding to collagen in the infarct region. GSL-NPs improved MI-induced heart failure in mice by inhibiting fibroblast fibrosis activation as well as protecting cardiomyocyte calcium homeostasis. Overall, we demonstrate a therapeutic approach that produces a superimposed protective effect in mice with MI through targeted delivery by nanoparticles.

Previous studies have shown that it is challenging to target damaged myocardium due to its histological properties and rapid hemodynamics [35,36]. Recently, there has been growing evidence that nanoparticle-based gene therapy is effective in treating myocardial infarction, myocardial ischemia/reperfusion injury, heart failure, and other cardiac diseases [37–39]. In this nanomedicine strategy, nanoparticles are modified using different targeting molecules to achieve cardiac-specific drug and gene delivery. Phage display technology is a technique that has emerged to discover tissue-specific targeting methods that can be sequenced and used as targeting molecules. GKWHCTTKFPHHYCL peptides are specific binding peptides for type I collagen, the primary collagen component in fibrotic myocardium, identified by in vivo phage display technology [40–42]. The novelty of the present study is that we tried to target damaged myocardium based on the pathological feature that myocardial damage gradually develops into fibrosis. The nanoparticles can be effectively targeted to damaged myocardial tissue to inhibit cardiac fibrosis and maintain cardiac calcium homeostasis by releasing the loaded plasmid DNA into cardiac fibroblasts and cardiomyocytes, which provides a new therapeutic idea for traditional post-myocardial infarction therapy.

It is considered that ischemia-induced myocardial contractile injury is the main cause triggering LV dysfunction during acute MI [43]. Calcium homeostasis regulated by ion channels plays a crucial role in maintaining the normal contraction of cardiomyocytes [6,44]. As a regulator of calcium homeostasis by driving calcium reuptake into the SR during diastole, Serca2a has been shown to be downregulated in damaged cardiomyocytes in the myocardial infarction area, which leads to local systolic inactivity, causing an imbalance in myocardial contractions and ultimately accelerating heart failure [45–47]. After the occurrence of myocardial infarction, the damaged cardiomyocytes in the infarct area are generally intertwined with the fibrosis-activated cardiac fibroblasts. In addition, many previous studies have also demonstrated extensive intercellular interactions between adjacent cardiac fibroblasts and cardiomyocytes: Impaired cardiomyocytes mediate and promote the fibroblast-to-myofibroblast transition through TGF-β, angiotensin II (Ang II) and IL-6 signaling [48–50]; The massive secretion and transport of extracellular vesicles also ensure adequate material exchange between adjacent cardiomyocytes and cardiac fibroblasts [51,52]. On account of that, we designed a Serca2a nanorobot delivery system to ensure the targeted delivery into the infarct area by searching activated cardiac fibroblasts after myocardial infarction, and thus the liposomes in the targeted area can be delivered simultaneously to cardiac fibroblasts and damaged cardiomyocytes. In the present study, we showed that GSL-NPs could significantly enrich infarct areas where cardiac fibroblasts and impaired cardiomyocytes coexist. We demonstrated that cardiomyocytes could well take up GSL-NPs and rescue the impaired calcium recovery capacity of the sarcoplasmic reticulum in hypoxia, which plays a significant role in maintaining calcium homeostasis in the damaged cardiomyocyte. Using high-resolution echocardiography, we further proved that GSL-NPs delivery significantly improved left ventricular systolic functions in MI mice, with these effects lasting up to 28 days. The above results suggest that administering a nanoparticle delivery system may benefit patients recovering from MI.

Excessive fibrosis in the infarct area is considered to be another reason providing the poor prognosis in patients who underwent acute MI [45]. Fibrotic activation after acute myocardial infarction serves as a reparative response to the ischemic insult in which the damaged heart tissue is replaced with a fibrous scar [53]. Although the scar is essential to prevent ventricular wall rupture in the early stages, as the fibrosis progresses, the expanded fibrosis area leads to cardiac structural disruptions and systolic myocardial dysfunctions [5,54,55]. Accumulating number of studies were trying to alleviate irreversible heart failure by regulating the fibrosis process after MI through multiple potential signaling [56–58]. Transforming growth factor-β1 (TGF-β1) is thought to be the core factor in the fibrotic process, which causes tissue-scarring primarily by activating its downstream SMAD2/3 complex to promote fibroblasts undergo myofibroblast transdifferentiation and produce extracellular matrix (ECM) [53,59]. The inflammatory signaling led by NF-κB also plays a role in promoting the process of cardiac fibrosis [60,61]. A recent study has shown that AAV1-delivered Serca2a alleviates TGF-β-induced pulmonary fibrosis by upstream blockade of the NF-κB signaling pathway [15]. However, given the rapidity of cardiac blood flow and the specificity of the heart, the AAV-mediated therapeutic system has shown its limitations in the treatment of MI. Concerns about AAV's biosafety also limit its clinical translation.

In this study, we demonstrated the safety of gene therapy via nanoparticle loading with no significant damage to mice, even at doses up to 1.0 mg/kg, and 1.0 mg/ml. In vitro CCK-8 and TUNEL assays further proved that treatment of GSL-NPs does no harm to normal H9C2s as well as cardiac fibroblasts within a dose of 2 mg/ml. In addition, due to the characteristics of high hemodynamics and the difficulty of specific enrichment of damaged cardiomyocytes, we designed the scheme that the liposome was the first to connect collagen fiber 1, which allowed it to be more significantly enriched in the infarct area. Therefore, besides the role of Serca2a itself in maintaining calcium homeostasis in cardiomyocytes, this nanomaterial delivery therapy can also effectively attenuate the process of the infarcted regions development by inhibiting fibrosis activation, as confirmed by Masson-staining and western blot assays. Through the additive effect of enhancing myocardial contraction and anti-fibrosis, nanoparticle-derived Serca2a gene therapy has achieved a multi-part integrated intervention mode of targeted delivery, multi-dimensional intervention, and precise attack, providing the possibility for the improvement of prognosis after MI with nano-gene technology.

There are several limitations should be highlighted in the present study. Despite the apparent therapeutic effect, a direct therapeutic comparison between the AAV-mediated and GSL-NPs-mediated delivery systems deserves to be conducted. In addition, we did not elucidate how Serca2a affects fibrosis progression in cardiac fibroblasts; although the down-regulation of NF-κB signaling was observed in mouse heart tissue, it still warrants further investigation due to the potential therapeutic value of Serca2a in the clinical practice. Third, based on our liposomal design, GSL-NPs will be significantly enriched in the infarct area during myocardial infarction fibrosis formation but may be unexpectedly enriched in other organs when there are significant fibrotic lesions, such as liver fibrosis or kidney fibrosis. Therefore, the risk of clinical transformation in patients with myocardial infarction combined with other fibrotic diseases needs to be further evaluated.

In conclusion, we conduct a nanorobot-mediated therapy system with high biosafety and high efficiency for myocardial infarction area targeted delivery. We demonstrated that GSL-NPs-mediated Serca2a gene therapy could alleviate MI-induced heart failure by maintaining myocardial calcium homeostasis and inhibiting excessive fibrosis activation.

Funding

The National Natural Science Foundation of China (Nos. 81974030), the Key Grant from the National Clinical Research Center for Child Health and Disorders (Nos. NCRCCHD-2021-KP-01), and the National Key Clinical Specialty.

CRediT authorship contribution statement

Wanshi Chen: Writing – original draft, Methodology, Formal analysis, Conceptualization. **Lingjuan Liu:** Writing – review & editing, Methodology, Formal analysis. **Ming Tang:** Methodology, Formal analysis. **Jiajin Li:** Methodology. **Wenjing Yuan:** Methodology. **Dan Yin:** Methodology. **Yang Cao:** Methodology. **Jie Tian:** Writing – review & editing, Funding acquisition.

Declaration of competing interest

The authors declare that they have no known competing financial interests or personal relationships that could have appeared to influence the work reported in this paper.

Data availability

The data that has been used is confidential.

Appendix A. Supplementary data

Supplementary data to this article can be found online at. https://doi.org/10.1016/j.mtbio.2024.101162.

References

[1] D. Jenča, V. Melenovský, J. Stehlik, V. Staněk, J. Kettner, J. Kautzner, V. Adámková, P. Wohlfahrt, Heart failure after myocardial infarction: incidence and predictors, ESC Heart Fail 8 (1) (2021) 222–237.

[2] M.W. Bloom, B. Greenberg, T. Jaarsma, J.L. Januzzi, C.S.P. Lam, A.P. Maggioni, J. N. Trochu, J. Butler, Heart failure with reduced ejection fraction, Nat. Rev. Dis. Prim. 3 (2017) 17058.

[3] B. Ibanez, S. James, S. Agewall, M.J. Antunes, C. Bucciarelli-Ducci, H. Bueno, A.L. P. Caforio, F. Crea, J.A. Goudevenos, S. Halvorsen, G. Hindricks, A. Kastrati, M. J. Lenzen, E. Prescott, M. Roffi, M. Valgimigli, C. Varenhorst, P. Vranckx, P. Widimský, ESC Guidelines for the management of acute myocardial infarction in patients presenting with ST-segment elevation: the Task Force for the management of acute myocardial infarction in patients presenting with ST-segment elevation of the European Society of Cardiology (ESC), Eur. Heart J. 39 (2) (2017) 119–177.

[4] D.P. Del Re, D. Amgalan, A. Linkermann, Q. Liu, R.N. Kitsis, Fundamental mechanisms of regulated cell death and implications for heart disease, Physiol. Rev. 99 (4) (2019) 1765–1817.

[5] S.D. Prabhu, N.G. Frangogiannis, The biological basis for cardiac repair after myocardial infarction: from inflammation to fibrosis, Circ. Res. 119 (1) (2016) 91–112.

[6] G. Morciano, A. Rimessi, S. Patergnani, V.A.M. Vitto, A. Danese, A. Kahsay, L. Palumbo, M. Bonora, M.R. Wieckowski, C. Giorgi, P. Pinton, Calcium dysregulation in heart diseases: targeting calcium channels to achieve a correct calcium homeostasis, Pharmacol. Res. 177 (2022) 106119.

[7] J. Goerg, M. Sommerfeld, B. Greiner, D. Lauer, Y. Seckin, A. Kulikov, D. Ivkin, U. Kintscher, S. Okovityi, E. Kaschina, Low-dose empagliflozin improves systolic heart function after myocardial infarction in rats: regulation of MMP9, NHE1, and SERCA2a, Int. J. Mol. Sci. 22 (11) (2021).

[8] B. Ning, X. Qi, Y. Li, H. Liu, F. Zhang, C. Qin, Biventricular pacing cardiac contractility modulation improves cardiac contractile function via upregulating SERCA2 and miR-133 in a rabbit model of congestive heart failure, Cell. Physiol. Biochem. 33 (5) (2014) 1389–1399.

[9] Y. Zhang, L. Jiao, L. Sun, Y. Li, Y. Gao, C. Xu, Y. Shao, M. Li, C. Li, Y. Lu, Z. Pan, L. Xuan, Y. Zhang, Q. Li, R. Yang, Y. Zhuang, Y. Zhang, B. Yang, LncRNA ZFAS1 as a SERCA2a inhibitor to cause intracellular Ca(2+) overload and contractile dysfunction in a mouse model of myocardial infarction, Circ. Res. 122 (10) (2018) 1354–1368.

[10] Y. Guo, J. Xu, Y. Deng, L. Wu, J. Wang, J. An, In vivo effects of nitrosyl hydrogen on cardiac function and sarcoplasmic reticulum calcium pump (SERCA2a) in rats with heart failure after myocardial infarction, Cardiovasc. Diagn. Ther. 10 (6) (2020) 1795–1804.

[11] M.A. Talukder, F. Yang, Y. Nishijima, C.A. Chen, A. Kalyanasundaram, M. Periasamy, J.L. Zweier, Reduced SERCA2a converts sub-lethal myocardial injury to infarction and affects postischemic functional recovery, J. Mol. Cell. Cardiol. 46 (2) (2009) 285–287.

[12] B. Ye, H. Zhou, Y. Chen, W. Luo, W. Lin, Y. Zhao, J. Han, X. Han, W. Huang, G. Wu, X. Wang, G. Liang, USP25 ameliorates pathological cardiac hypertrophy by stabilizing SERCA2a in cardiomyocytes, Circ. Res. 132 (4) (2023) 465–480.

[13] Y. Hu, C. Zhang, H. Zhu, S. Wang, Y. Zhou, J. Zhao, Y. Xia, D. Li, Luteolin modulates SERCA2a via Sp1 upregulation to attenuate myocardial ischemia/reperfusion injury in mice, Sci. Rep. 10 (1) (2020) 15407.

[14] K. Niwano, M. Arai, N. Koitabashi, A. Watanabe, Y. Ikeda, H. Miyoshi, M. Kurabayashi, Lentiviral vector-mediated SERCA2 gene transfer protects against heart failure and left ventricular remodeling after myocardial infarction in rats, Mol. Ther. : the journal of the American Society of Gene Therapy 16 (6) (2008) 1026–1032.

[15] M. Bisserier, J. Milara, Y. Abdeldjebbar, S. Gubara, C. Jones, C. Bueno-Beti, E. Chepurko, E. Kohlbrenner, M.G. Katz, S. Tarzami, J. Cortijo, J. Leopold, R. J. Hajjar, Y. Sassi, L. Hadri, AAV1.SERCA2a gene therapy reverses pulmonary fibrosis by blocking the STAT3/FOXM1 pathway and promoting the SNON/SKI Axis, Mol. Ther. : the journal of the American Society of Gene Therapy 28 (2) (2020) 394–410.

[16] H. Khalil, O. Kanisicak, V. Prasad, R.N. Correll, X. Fu, T. Schips, R.J. Vagnozzi, R. Liu, T. Huynh, S.J. Lee, J. Karch, J.D. Molkentin, Fibroblast-specific TGF-β-Smad2/3 signaling underlies cardiac fibrosis, J. Clin. Invest. 127 (10) (2017) 3770–3783.

[17] S.A. Su, D. Yang, Y. Wu, Y. Xie, W. Zhu, Z. Cai, J. Shen, Z. Fu, Y. Wang, L. Jia, Y. Wang, J.A. Wang, M. Xiang, EphrinB2 regulates cardiac fibrosis through modulating the interaction of Stat3 and TGF-β/Smad3 signaling, Circ. Res. 121 (6) (2017) 617–627.

[18] Q. Zhang, L. Wang, S. Wang, H. Cheng, L. Xu, G. Pei, Y. Wang, C. Fu, Y. Jiang, C. He, Q. Wei, Signaling pathways and targeted therapy for myocardial infarction, Signal Transduct. Targeted Ther. 7 (1) (2022) 78.

[19] P. Wu, Y. Zhai, D. Li, The function and significance of SERA2a in congestive heart failure: an analysis of gene therapy trials, Histol. Histopathol. 32 (8) (2017) 767–777.

[20] I. Warbrick, S.W. Rabkin, Effect of the peptides Relaxin, Neuregulin, Ghrelin and Glucagon-like peptide-1, on cardiomyocyte factors involved in the molecular mechanisms leading to diastolic dysfunction and/or heart failure with preserved ejection fraction, Peptides 111 (2019) 33–41.

[21] B. Greenberg, J. Butler, G.M. Felker, P. Ponikowski, A.A. Voors, A.S. Desai, D. Barnard, A. Bouchard, B. Jaski, A.R. Lyon, J.M. Pogoda, J.J. Rudy, K.M. Zsebo, Calcium upregulation by percutaneous administration of gene therapy in patients with cardiac disease (CUPID 2): a randomised, multinational, double-blind, placebo-controlled, phase 2b trial, Lancet (London, England) 387 (10024) (2016) 1178–1186.

[22] X. Chen, Y. Zhang, H. Zhang, L. Zhang, L. Liu, Y. Cao, H. Ran, J. Tian, A non-invasive nanoparticles for multimodal imaging of ischemic myocardium in rats, J. Nanobiotechnol. 19 (1) (2021) 82.

[23] Y. Zhang, X. Chen, L. Liu, J. Tian, L. Hao, H.T. Ran, Photoacoustic imaging of myocardial infarction region using non-invasive fibrin-targeted nanoparticles in a rat myocardial ischemia-reperfusion model, Int. J. Nanomed. 16 (2021) 1331–1344.

[24] P. Caravan, B. Das, S. Dumas, F.H. Epstein, P.A. Helm, V. Jacques, S. Koerner, A. Kolodziej, L. Shen, W.C. Sun, Z. Zhang, Collagen-targeted MRI contrast agent for molecular imaging of fibrosis, Angew. Chem. 46 (43) (2007) 8171–8173.

[25] L. Ledsgaard, A. Ljungars, C. Rimbault, C.V. Sørensen, T. Tulika, J. Wade, Y. Wouters, J. McCafferty, A.H. Laustsen, Advances in antibody phage display technology, Drug Discov. Today 27 (8) (2022) 2151–2169.

[26] M. Tang, L. Hong, H. Li, W. Chen, L. Tai, R. Minshall, W. Huang, J. Chen, Stiffness of aortic arch and carotid arteries increases in ApoE-knockout mice with high-fat diet: evidence from echocardiography, Am. J. Tourism Res. 13 (3) (2021) 1352–1364.

[27] D. Yang, M. Tang, M. Zhang, H. Ren, X. Li, Z. Zhang, B. He, S. Peng, W. Wang, D. Fang, Y. Song, Y. Xiong, Z.Z. Liu, L. Liang, W. Shi, C. Fu, Y. Hu, P.A. Jose, L. Zhou, Y. Han, C. Zeng, Downregulation of G protein-coupled receptor kinase 4 protects against kidney ischemia-reperfusion injury, Kidney Int. 103 (4) (2023) 719–734.

[28] W.E. Wang, L. Li, X. Xia, W. Fu, Q. Liao, C. Lan, D. Yang, H. Chen, R. Yue, C. Zeng, L. Zhou, B. Zhou, D.D. Duan, X. Chen, S.R. Houser, C. Zeng, Dedifferentiation, proliferation, and redifferentiation of adult mammalian cardiomyocytes after ischemic injury, Circulation 136 (9) (2017) 834–848.

[29] Q. Lu, B. Pan, H. Bai, W. Zhao, L. Liu, G. Li, R. Liu, T. Lv, X. Huang, X. Li, J. Tian, Intranuclear cardiac troponin I plays a functional role in regulating Atp2a2 expression in cardiomyocytes, Genes & diseases 9 (6) (2022) 1689–1700.

[30] N. Enzan, S. Matsushima, S. Ikeda, K. Okabe, A. Ishikita, T. Yamamoto, M. Sada, R. Miyake, Y. Tsutsui, R. Nishimura, T. Toyohara, Y. Ikeda, Y. Shojima, H. D. Miyamoto, T. Tadokoro, M. Ikeda, K. Abe, T. Ide, S. Kinugawa, H. Tsutsui, ZBP1 protects against mtDNA-induced myocardial inflammation in failing hearts, Circ. Res. 132 (9) (2023) 1110–1126.

[31] F. Hua, J.Y. Li, M. Zhang, P. Zhou, L. Wang, T.J. Ling, G.H. Bao, Kaempferol-3-O-rutinoside exerts cardioprotective effects through NF-κB/NLRP3/Caspase-1 pathway in ventricular remodeling after acute myocardial infarction, J. Food Biochem. 46 (10) (2022) e14305.

[32] J. Feng, J. Zhan, S. Ma, LRG1 promotes hypoxia-induced cardiomyocyte apoptosis and autophagy by regulating hypoxia-inducible factor-1α, Bioengineered 12 (1) (2021) 8897–8907.

[33] Y. Li, S. Ren, J. Xia, Y. Wei, Y. Xi, EIF4A3-Induced circ-BNIP3 aggravated hypoxia-induced injury of H9c2 cells by targeting miR-27a-3p/BNIP3, Mol. Ther. Nucleic Acids 19 (2020) 533–545.

[34] S. Li, Y. Chen, Y. Jia, T. Xue, X. Hou, Z. Zhao, Transcription factor JDP2 activates PDE4B to participate in hypoxia/reoxygenation-induced H9c2 cell injury, Exp. Ther. Med. 23 (5) (2022) 340.

[35] M. Cheraghi, B. Negahdari, H. Daraee, A. Eatemadi, Heart targeted nanoliposomal/nanoparticles drug delivery: an updated review, Biomedicine & pharmacotherapy = Biomedecine & pharmacotherapie 86 (2017) 316–323.

[36] H. Omidian, N. Babanejad, L.X. Cubeddu, Nanosystems in cardiovascular medicine: advancements, applications, and future perspectives, Pharmaceutics 15 (7) (2023).

[37] T. Zhao, W. Wu, L. Sui, Q. Huang, Y. Nan, J. Liu, K. Ai, Reactive oxygen species-based nanomaterials for the treatment of myocardial ischemia reperfusion injuries, Bioact. Mater. 7 (2022) 47–72.
[38] H. Li, J. Zhu, Y.W. Xu, F.F. Mou, X.L. Shan, Q.L. Wang, B.N. Liu, K. Ning, J.J. Liu, Y. C. Wang, J.X. Mi, X. Wei, S.J. Shao, G.H. Cui, R. Lu, H.D. Guo, Notoginsenoside R1-loaded mesoporous silica nanoparticles targeting the site of injury through inflammatory cells improves heart repair after myocardial infarction, Redox Biol. 54 (2022) 102384.
[39] M. Miragoli, P. Ceriotti, M. Iafisco, M. Vacchiano, N. Salvarani, A. Alogna, P. Carullo, G.B. Ramirez-Rodríguez, T. Patrício, L.D. Esposti, F. Rossi, F. Ravanetti, S. Pinelli, R. Alinovi, M. Erreni, S. Rossi, G. Condorelli, H. Post, A. Tampieri, D. Catalucci, Inhalation of peptide-loaded nanoparticles improves heart failure, Sci. Transl. Med. 10 (424) (2018).
[40] K. Nagano, Y. Tsutsumi, Phage display technology as a powerful platform for antibody drug discovery, Viruses 13 (2) (2021).
[41] K. Pierzynowska, J. Morcinek-Orłowska, L. Gaffke, W. Jaroszewicz, P.M. Skowron, G. Węgrzyn, Applications of the phage display technology in molecular biology, biotechnology and medicine, Crit. Rev. Microbiol. (2023) 1–41.
[42] I.Y. Zhou, O.A. Catalano, P. Caravan, Advances in functional and molecular MRI technologies in chronic liver diseases, J. Hepatol. 73 (5) (2020) 1241–1254.
[43] M.G. Del Buono, F. Moroni, R.A. Montone, L. Azzalini, T. Sanna, A. Abbate, Ischemic cardiomyopathy and heart failure after acute myocardial infarction, Curr. Cardiol. Rep. 24 (10) (2022) 1505–1515.
[44] T.S. Shankar, D.K.A. Ramadurai, K. Steinhorst, S. Sommakia, R. Badolia, A. Thodou Krokidi, D. Calder, S. Navankasattusas, P. Sander, O.S. Kwon, A. Aravamudhan, J. Ling, A. Dendorfer, C. Xie, O. Kwon, E.H.Y. Cheng, K.J. Whitehead, T. Gudermann, R.S. Richardson, F.B. Sachse, J. Schredelseker, K.W. Spitzer, D. Chaudhuri, S.G. Drakos, Cardiac-specific deletion of voltage dependent anion channel 2 leads to dilated cardiomyopathy by altering calcium homeostasis, Nat. Commun. 12 (1) (2021) 4583.
[45] M. Holmes, M.E. Hurley, T.M.D. Sheard, A.P. Benson, I. Jayasinghe, M.A. Colman, Increased SERCA2a sub-cellular heterogeneity in right-ventricular heart failure inhibits excitation-contraction coupling and modulates arrhythmogenic dynamics, Philos. Trans. R. Soc. Lond. B Biol. Sci. 377 (1864) (2022) 20210317.
[46] I. Ragone, J. Barallobre-Barreiro, K. Takov, K. Theofilatos, X. Yin, L.E. Schmidt, N. Domenech, M.G. Crespo-Leiro, S.M. van der Voorn, A. Vink, T.A.B. van Veen, C. Bödör, B. Merkely, T. Radovits, M. Mayr, SERCA2a protein levels are unaltered in human heart failure, Circulation 148 (7) (2023) 613–616.
[47] S. Sarma, J.P. MacNamara, M. Hieda, E.J. Howden, J.S. Lawley, S. Livingston, M. Samels, B.D. Levine, SERCA2a agonist effects on cardiac performance during exercise in heart failure with preserved ejection fraction, JACC Heart Fail 11 (7) (2023) 760–771.
[48] C. Hall, K. Gehmlich, C. Denning, D. Pavlovic, Complex relationship between cardiac fibroblasts and cardiomyocytes in Health and disease, J. Am. Heart Assoc. 10 (5) (2021) e019338.
[49] L. Hecker, R. Jagirdar, T. Jin, V.J. Thannickal, Reversible differentiation of myofibroblasts by MyoD, Exp. Cell Res. 317 (13) (2011) 1914–1921.
[50] J. Pellman, J. Zhang, F. Sheikh, Myocyte-fibroblast communication in cardiac fibrosis and arrhythmias: mechanisms and model systems, J. Mol. Cell. Cardiol. 94 (2016) 22–31.
[51] J. Li, A.M. Salvador, G. Li, N. Valkov, O. Ziegler, A. Yeri, C. Yang Xiao, B. Meechoovet, E. Alsop, R.S. Rodosthenous, P. Kundu, T. Huan, D. Levy, J. Tigges, A.R. Pico, I. Ghiran, M.G. Silverman, X. Meng, R. Kitchen, J. Xu, K. Van Keuren-Jensen, R. Shah, J. Xiao, S. Das, Mir-30d regulates cardiac remodeling by intracellular and paracrine signaling, Circ. Res. 128 (1) (2021) e1–e23.
[52] S. Fu, Y. Zhang, Y. Li, L. Luo, Y. Zhao, Y. Yao, Extracellular vesicles in cardiovascular diseases, Cell death discovery 6 (2020) 68.
[53] J. Yuan, H. Yang, C. Liu, L. Shao, H. Zhang, K. Lu, J. Wang, Y. Wang, Q. Yu, Y. Zhang, Y. Yu, Z. Shen, Microneedle patch loaded with exosomes containing MicroRNA-29b prevents cardiac fibrosis after myocardial infarction, Adv. Healthcare Mater. 12 (13) (2023) e2202959.
[54] S. Frantz, M.J. Hundertmark, J. Schulz-Menger, F.M. Bengel, J. Bauersachs, Left ventricular remodelling post-myocardial infarction: pathophysiology, imaging, and novel therapies, Eur. Heart J. 43 (27) (2022) 2549–2561.
[55] H. Gil, M. Goldshtein, S. Etzion, S. Elyagon, U. Hadad, Y. Etzion, S. Cohen, Defining the timeline of periostin upregulation in cardiac fibrosis following acute myocardial infarction in mice, Sci. Rep. 12 (1) (2022) 21863.
[56] H. Tani, T. Sadahiro, Y. Yamada, M. Isomi, H. Yamakawa, R. Fujita, Y. Abe, T. Akiyama, K. Nakano, Y. Kuze, M. Seki, Y. Suzuki, M. Fujisawa, M. Sakata-Yanagimoto, S. Chiba, K. Fukuda, M. Ieda, Direct reprogramming improves cardiac function and reverses fibrosis in chronic myocardial infarction, Circulation 147 (3) (2023) 223–238.
[57] A. Han, Y. Lu, Q. Zheng, J. Zhang, Y. Zhao, M. Zhao, X. Cui, Qiliqiangxin attenuates cardiac remodeling via inhibition of TGF-β1/smad3 and NF-κB signaling pathways in a rat model of myocardial infarction, Cell. Physiol. Biochem. 45 (5) (2018) 1797–1806.
[58] S.A. Bageghni, K.E. Hemmings, N.Y. Yuldasheva, A. Maqbool, F.O. Gamboa-Esteves, N.E. Humphreys, M.S. Jackson, C.P. Denton, S. Francis, K.E. Porter, J. F. Ainscough, E. Pinteaux, M.J. Drinkhill, N.A. Turner, Fibroblast-specific deletion of interleukin-1 receptor-1 reduces adverse cardiac remodeling following myocardial infarction, JCI insight 5 (17) (2019).
[59] S. Song, R. Zhang, W. Cao, G. Fang, Y. Yu, Y. Wan, C. Wang, Y. Li, Q. Wang, Foxm1 is a critical driver of TGF-β-induced EndMT in endothelial cells through Smad2/3 and binds to the Snail promoter, J. Cell. Physiol. 234 (6) (2019) 9052–9064.
[60] K. Liu, J. Wang, X. Gao, W. Ren, C1q/TNF-Related protein 9 inhibits coxsackievirus B3-induced injury in cardiomyocytes through NF-κB and TGF-β1/smad2/3 by modulating THBS1, Mediat. Inflamm. 2020 (2020) 2540687.
[61] L.X. Zou, C. Chen, X. Yan, Q.Y. Lin, J. Fang, P.B. Li, X. Han, Q.S. Wang, S.B. Guo, H. H. Li, Y.L. Zhang, Resveratrol attenuates pressure overload-induced cardiac fibrosis and diastolic dysfunction via PTEN/AKT/Smad2/3 and NF-κB signaling pathways, Mol. Nutr. Food Res. 63 (24) (2019) e1900418.